Inorganic Materials, Vol. 41, No. 1, 2005, pp. 87–93. Translated from Neorganicheskie Materialy, Vol. 41, No. 1, 2005, pp. 93–100.

Oxidation of Reduced Y-Doped Semiconducting Barium Titanate Ceramics

O. I. V'yunov, L. L. Kovalenko, A. G. Belous, and V. N. Belyakov

Vernadsky Institute of General and Inorganic Chemistry, National Academy of Sciences of Ukraine, pr. Akademika Palladina 32/34, Kiev, 03680 Ukraine

e-mail: vyunov@ionc.kar.net

Received February 27, 2004

Abstract—Oxidation-induced microstructural changes in reduced yttrium-doped barium titanate ($Ba_{1-x}Y_x^{\bullet}Ti_{1-x}^{4+}Ti_x^{3+}O_3$) are studied using samples sintered in a reducing atmosphere ($p_{O_2} = 10^{-4}$ Pa) and then oxidized in air at 1150 and 1350°C. The results indicate that oxidation leads to precipitation of $Ba_6Ti_{17}O_{40}$ and, at relatively high doping levels, $Y_2Ti_2O_7$. These phases increase the electrical resistance of the outer layer of the grains in the ceramics.

INTRODUCTION

Donor-doped polycrystalline barium titanate sintered in air possesses semiconducting properties in a narrow range of doping levels and has a positive temperature coefficient of resistance (PTCR), a feature of great practical importance. Semiconducting properties can be imparted to barium titanate by doping with rare earths (e.g., with Y, La, and Nd) on the Ba site [1, 2] or with group V and VI metals (e.g., Nb, Ta, and Mo) on the Ti site [3, 4]. The semiconducting phase resulting from doping with rare earths, e.g., with yttrium, can be represented by the general formula $Ba_{1-x}Y_x^{\bullet}Ti_{1-x}^{4+}Ti_x^{3+}O_3$ [5]. Hereafter, we use Kröger notation [6]: $Y^{\bullet}$ stands for an yttrium ion in the Ba site (excess positive charge 1+), and V_{Ti}'''' is a Ti vacancy (excess negative charge 4–). Postsintering cooling may be accompanied by grain-boundary oxidation, resulting in oxidized barium titanate, a dielectric material containing cation vacancies, which compensate the excess charge introduced by donor doping [7]. As shown by Buskaglia *et al.* [8] in an atomistic simulation study of doping processes, the energy of formation of the $Y_{Ba}^{\bullet} + V_{Ti}''''$ defect complex (4.35 eV) is lower than that for $Y_{Ba}^{\bullet} + V_{Ba}''$ (7.23 eV). Consequently, oxidized Y-doped barium titanate can be represented by the general formula $Ba_{1-x}Y_x^{\bullet}Ti_{1-x/4}^{4+}(V_{Ti}'''')_{x/4}O_3$ [7].

Grain-boundary oxidation processes during sintering and subsequent cooling in air are known to play an important role in determining the PTCR behavior of ceramics. These processes are difficult to investigate by x-ray diffraction (XRD) because the yttrium content of barium titanate is typically at a level of a few tenths of a percent and because oxidation occurs, as a rule, in a thin surface layer of the grains. To gain insight into grain-boundary processes, a number of studies were concerned with oxidation of fine-particle reduced barium titanate [7]. The use of fine powders markedly increases the oxidation surface and, accordingly, the content of the resulting phases, which allows these phases to be identified by XRD. It is well known [9] that synthesis in a reducing atmosphere notably extends the composition range of substitutional solid solutions of rare-earth ions in barium titanate compared to synthesis in air. Therefore, studying reoxidized barium titanate, one can gain information about the phases forming at grain boundaries at low rare-earth concentrations (at which samples synthesized in air exhibit PTCR behavior) and high rare-earth concentrations (at which samples synthesized in air are possess dielectric properties and exhibit no PTCR behavior). This approach was used by Makovec and Drofenik [7] to investigate the microstructural changes during the oxidation of reduced La-doped barium titanate.

In this paper, we describe microstructural changes accompanying the oxidation of reduced Y-doped barium titanate ($Ba_{1-x}Y_x^{\bullet}Ti_{1-x}^{4+}Ti_x^{3+}O_3$) and impedance measurements carried out with the aim of elucidating the grain-boundary processes taking place during the synthesis of $BaTiO_3$-based PTCR materials.

EXPERIMENTAL

$Ba_{1-x}Y_x^{\bullet}Ti_{1-x}^{4+}Ti_x^{3+}O_3$ ceramics were prepared by solid-state reactions. Appropriate amounts of extra-pure-grade $BaCO_3$, TiO_2, and Y_2O_3 were mixed by grinding in an agate ball mill. After addition of 10% aqueous poly(vinyl alcohol), the mixtures were granu-

0020-1685/05/4101-0087

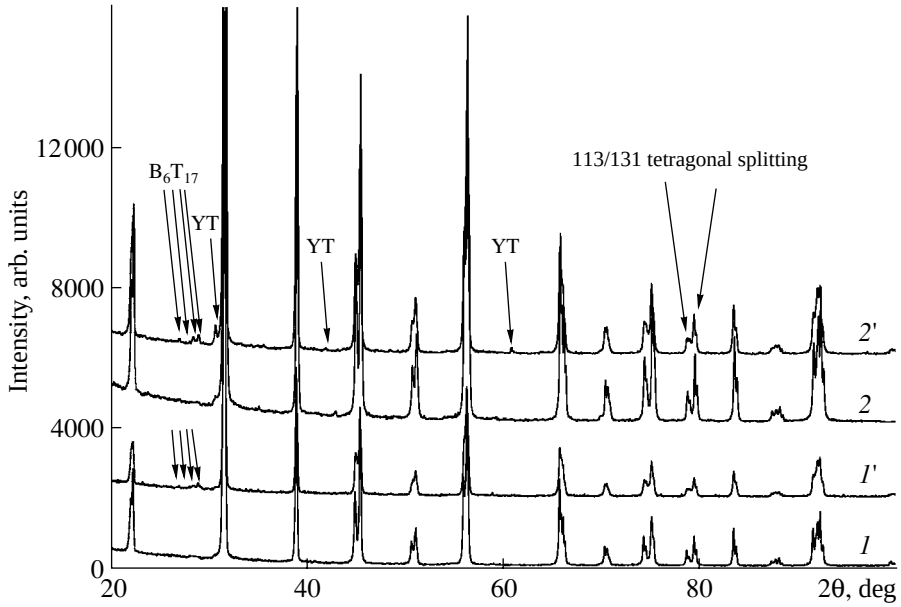

Fig. 1. XRD patterns of Y-doped barium titanate samples with the nominal compositions (*1*, *1*') $Ba_{0.99}Y_{0.01}Ti^{4+}_{0.99}Ti^{3+}_{0.01}O_3$ and (*2*, *2*') $Ba_{0.975}Y_{0.025}Ti^{4+}_{0.975}Ti^{3+}_{0.025}O_3$ after (*1*, *2*) sintering in a reducing atmosphere ($p_{O_2} = 10^{-4}$ Pa) and (*1*', *2*') and subsequent oxidation in air for 20 h at 1150°C; $B_6T_{17} = Ba_6Ti_{17}O_{40}$, YT = $Y_2Ti_2O_7$.

lated and then pressed at 150 MPa into pellets 10 mm in diameter and ≈2 mm in thickness, which were sintered at 1400°C in a reducing atmosphere ($p_{O_2} = 10^{-4}$ Pa). Under such conditions, the Y solubility in the Ba sublattice attains 4 at % [9], whereas the Y content of materials sintered in air is no higher than 1.5 at % [10]. In studies of oxidation processes, we used samples with $x = 0.01$ (below the solubility limit of Y in the Ba sublattice in air) and 0.025 (above the Y solubility in the Ba sublattice in air but below that at $p_{O_2} = 10^{-4}$ Pa). The cation stoichiometry determined by wavelength-dispersive x-ray microanalysis agreed well with the nominal compositions of the samples. We oxidized both pellets and powder samples prepared by grinding pellets, followed by screening through a 400-mesh nylon-6 sieve. Oxidation was carried out at 1150 and 1350°C for 20 and 1 h, respectively. The phase composition of the powders was determined by XRD on a DRON-4-07 diffractometer (CuK_α radiation, 40 kV, 20 mA). The pellets were examined by electron microscopy.

Dielectric properties in the microwave region (1 GHz) were studied on cylindrical samples 1 mm in diameter and 1 mm in height, using a coaxial line. Dielectric permittivity was evaluated as described elsewhere [11]. In impedance measurements, we used a Solartron PGSTAT-30 impedance analyzer in the range 100 Hz to 1 MHz and a VM-560 Q-meter in the range 50 kHz to 35 MHz. The components of the equivalent circuit were identified using the Frequency Response Analyser 4.7 program.

RESULTS AND DISCUSSION

Figure 1 shows the XRD patterns of samples with the nominal compositions $Ba_{0.99}Y_{0.01}Ti^{4+}_{0.99}Ti^{3+}_{0.01}O_3$ and $Ba_{0.975}Y_{0.025}Ti^{4+}_{0.975}Ti^{3+}_{0.025}O_3$ sintered in a reducing atmosphere ($p_{O_2} = 10^{-4}$ Pa) and then oxidized in air for 20 h at 1150°C. Both before and after oxidation, the samples had a tetragonally distorted structure (sp. gr. *P*4*mm* [12]).

As a result of oxidation at 1150°C for 20 h, the surface layer of the pellets turned light, attesting to $Ti^{3+} \longrightarrow Ti^{4+}$ oxidation, whereas the interior of the pellets remained dark, characteristic of the reduced material. Moreover, the sample interior was single-phase, whereas the surface layer of the oxidized samples was multiphase. In addition to the perovskite phase, it contained the pyrochlore phase $Y_2Ti_2O_7$ (sp. gr. $Fd\bar{3}m$, no. 227 [13]) and the monoclinic phase $Ba_6Ti_{17}O_{40}$ (sp. gr. *C*2/*c*, no. 15 [14]).

To assess the effect of yttrium on the temperature of the ferroelectric phase transition, we carried out dielectric measurements on $BaTiO_3$, $Ba_{0.99}Y_{0.01}Ti^{4+}_{0.99}Ti^{3+}_{0.01}O_3$, and $Ba_{0.975}Y_{0.025}Ti^{4+}_{0.975}Ti^{3+}_{0.025}O_3$ samples in the microwave region (1 GHz), where the effect of conductivity

is insignificant (Fig. 2). Comparison of the curves in Fig. 2a indicates that sintering of undoped $BaTiO_3$ in a reducing atmosphere shifts the peak in ε_{max} to lower temperatures and broadens it in comparison with air oxidation, which seems to be due to the development of lattice strain as a result of the formation of oxygen vacancies and to partial $Ti^{4+} \longrightarrow Ti^{3+}$ reduction, respectively [15]. Clearly, these processes in undoped barium titanate are interrelated.

Yttrium doping of $BaTiO_3$ further increases the width of the peak in $\varepsilon(t)$, for both the reduced and oxidized materials (Figs. 2b, 2c), which is characteristic of nonferroelectric impurities in ferroelectrics [16]. At the same time, in contrast to undoped $BaTiO_3$, we observe an insignificant shift of the peak in ε in going from the reduced (curves *1*) to the oxidized samples (curves *1'*). This indicates that the broadening of the peak is mainly due to the partial titanium reduction upon Y substitution on the Ba site. After sintering in a reducing atmosphere, the Y-doped barium titanate samples contain no oxygen vacancies or much lower concentrations of oxygen vacancies compared to undoped barium titanate [17], which accounts for the insignificant shift of the peak in $\varepsilon(t)$.

The present results indicate that, in reduced barium titanate, the excess charge introduced by Y doping is neutralized owing to partial $Ti^{4+} \longrightarrow Ti^{3+}$ reduction. During heat treatment of $Ba_{1-x}Y_x^{\bullet}Ti_{1-x}^{4+}Ti_x^{3+}O_3$ in an oxidizing atmosphere, charge compensation is due to the formation of Ti vacancies, accompanied by the precipitation of a Ti-rich phase:

$$Ba_{1-x}Y_xTi_{1-x}^{4+}Ti_x^{3+}O_3 + \frac{x}{4}O_2$$

$$\longrightarrow \frac{x}{y}Ba_{1-x}Y_xTi_{1-x/4}^{4+}(V_{Ti}'''')_{x/4}O_3 + \frac{x}{44}Ba_6Ti_{17}O_{40},$$

where $y = x\left(1 - \frac{3}{22}x\right)$.

This mechanism of charge compensation is operative at low doping levels (no higher than the yttrium solubility under oxidizing conditions).

If the doping level exceeds the yttrium solubility, oxidation leads to the precipitation of both $Ba_6Ti_{17}O_{40}$ and $Y_2Ti_2O_7$, and the process can be represented by the scheme

$$Ba_{1-(x+x_c)}Y_{x+x_c}Ti_{1-(x+x_c)}^{4+}Ti_{x+x_c}^{3+}O_3 + \frac{x+x_c}{4}O_2$$

$$\longrightarrow (1-z)\frac{x_c}{y}Ba_{1-x_c}Y_{x_c}Ti_{1-x_c/4}^{4+}(V_{Ti}'''')_{x_c/4}O_3$$

$$+ \frac{x_c}{44}Ba_6Ti_{17}O_{40} + \frac{z}{2}Y_2Ti_2O_7,$$

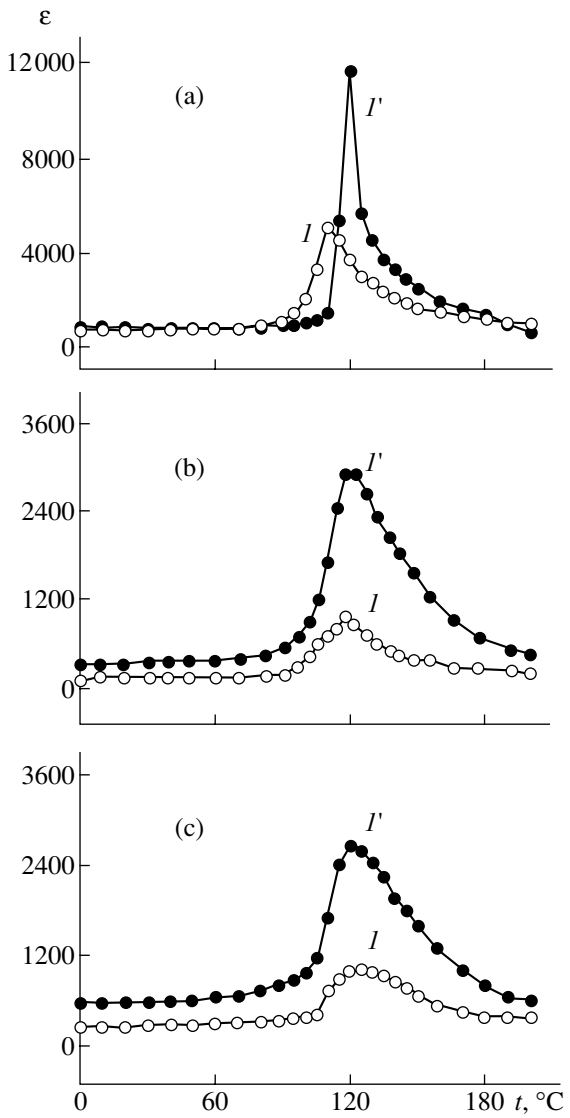

Fig. 2. Temperature dependences of 1-GHz dielectric permittivity for (a) $BaTiO_3$, (b) $Ba_{0.99}Y_{0.01}Ti_{0.99}^{4+}Ti_{0.01}^{3+}O_3$, and (c) $Ba_{0.975}Y_{0.025}Ti_{0.975}^{4+}Ti_{0.025}^{3+}O_3$ after (*1*) sintering in a reducing atmosphere ($p_{O_2} = 10^{-4}$ Pa) and (*1'*) subsequent air oxidation at 1150°C for 20 h.

where $y = x_c\left(1 - \frac{3}{22}x_c\right)$ and $z = x/(1 - x_c)$.

Figure 3 shows the semilog plots of resistivity versus temperature for materials synthesized in vacuum and then oxidized at high temperatures in air. The resistivity of the samples sintered in a reducing atmosphere decreases with increasing temperature. After oxidation, the $\rho(t)$ curves show regions of PTCR behavior.

Complex impedance and electric modulus measurements over a broad frequency range indicate that doped PTCR barium titanate ceramics consist of semicon-

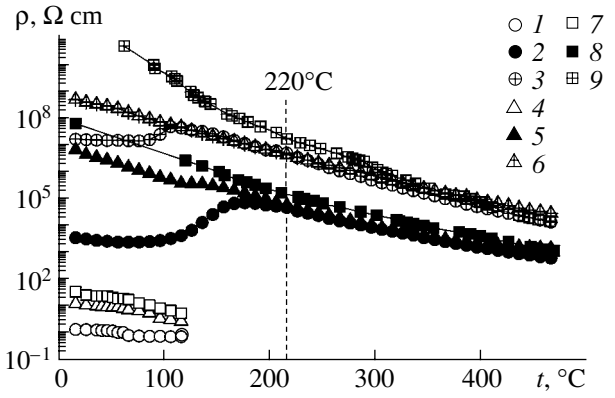

Fig. 3. Semilog plots of resistivity vs. temperature for (*1–3*) $Ba_{0.99}Y_{0.01}Ti^{4+}_{0.99}Ti^{3+}_{0.01}O_3$, (*4–6*) $Ba_{0.975}Y_{0.025}Ti^{4+}_{0.975}Ti^{3+}_{0.025}O_3$, and (*7–9*) $Ba_{0.96}Y_{0.04}Ti^{4+}_{0.96}Ti^{3+}_{0.04}O_3$ after (*1*, *4*, *7*) sintering in a reducing atmosphere ($p_{O_2} = 10^{-4}$ Pa) and subsequent air oxidation at (*2*, *5*, *8*) 1150 and (*3*, *6*, *9*) 1350°C.

ducting grains, with a higher resistance outer layer and high-resistance grain boundaries [18–20]. This structure can be represented by an equivalent circuit comprising three parallel *RC* circuits connected in series [20].

Dielectric properties can be analyzed in the form of the frequency dependences of complex impedance Z^*, complex admittance Y^*, complex permittivity ε^*, and complex electric modulus M^* [18–22]. These quantities are related by

$$M^* = 1/\varepsilon^* = i\omega C_0 Z^* = i\omega C_0(1/Y^*).$$

Data for PTCR materials are commonly represented as plots of Z'' versus Z', which are convenient for identifying the components of the equivalent circuit. In analyzing complex impedance data, use is also made of the frequency dependences of Z'' and M''. For a parallel *RC* circuit, the frequency dependences of Z'' and M'' have the form [18–22]

$$Z'' = R\frac{\omega RC}{1 + (\omega RC)^2}, \quad (1)$$

$$M'' = \frac{\varepsilon_0}{C}\frac{\omega RC}{1 + (\omega RC)^2}, \quad (2)$$

where $\omega = 2\pi f$ (f is frequency, Hz) and $\varepsilon_0 = 8.854 \times 10^{-14}$ F/cm is the permittivity of vacuum.

Equations (1) and (2) indicate that the frequency dependence of Z'' is sensitive to R (in our case, grain-boundary resistance), while that of M'' is influenced by the capacitance in the *RC* circuit (the capacitance of the grain bulk and surface layer) [18–20].

Parameters of peaks in the Nyquist diagrams for $BaTiO_3$-based ceramics oxidized in air at 1150 and 1350°C

Composition	f_{max}, Hz	R, kΩ ($R \approx 2Z''_{max}$)	Q, nF ($Q \approx \frac{1}{\omega_{max}R}$)	n	f_{max}, Hz	Q, nF ($Q \approx \frac{1}{2M''_{max}}$)	R, kΩ ($R \approx \frac{1}{\omega_{max}Q}$)	n	f_{max}, Hz	R_{total}, kΩ
	$Z''(f)$ (grain boundaries)				$M''(f)$ (outer layer of the grains)				$M''(f)$ (grain bulk)	
1150°C										
$Ba_{0.99}Y_{0.01}Ti^{4+}_{0.99}Ti^{3+}_{0.01}O_3$	500	8.0	30	0.87	–	–	–	–	$>10^6$	8.0
$Ba_{0.975}Y_{0.025}Ti^{4+}_{0.975}Ti^{3+}_{0.025}O_3$	360	8.6	29	0.78	15000	4.6	0.5	0.89	$>10^6$	9.1
$Ba_{0.96}Y_{0.04}Ti^{4+}_{0.96}Ti^{3+}_{0.04}O_3$	100	10.1	27	0.77	21000	2.8	1.1	0.89	$>10^6$	11.2
1350°C										
$Ba_{0.99}Y_{0.01}Ti^{4+}_{0.99}Ti^{3+}_{0.01}O_3$	$<10^2$	630	5.2	0.94	3800	2.8	11	0.90	$>10^6$	830
$Ba_{0.975}Y_{0.025}Ti^{4+}_{0.975}Ti^{3+}_{0.025}O_3$	$<10^2$	890	4.8	0.92	5300	0.5	53	0.87	$>10^6$	970
$Ba_{0.96}Y_{0.04}Ti^{4+}_{0.96}Ti^{3+}_{0.04}O_3$	$<10^2$	1700	4.6	0.90	14000	0.1	85	0.77	$>10^6$	2270

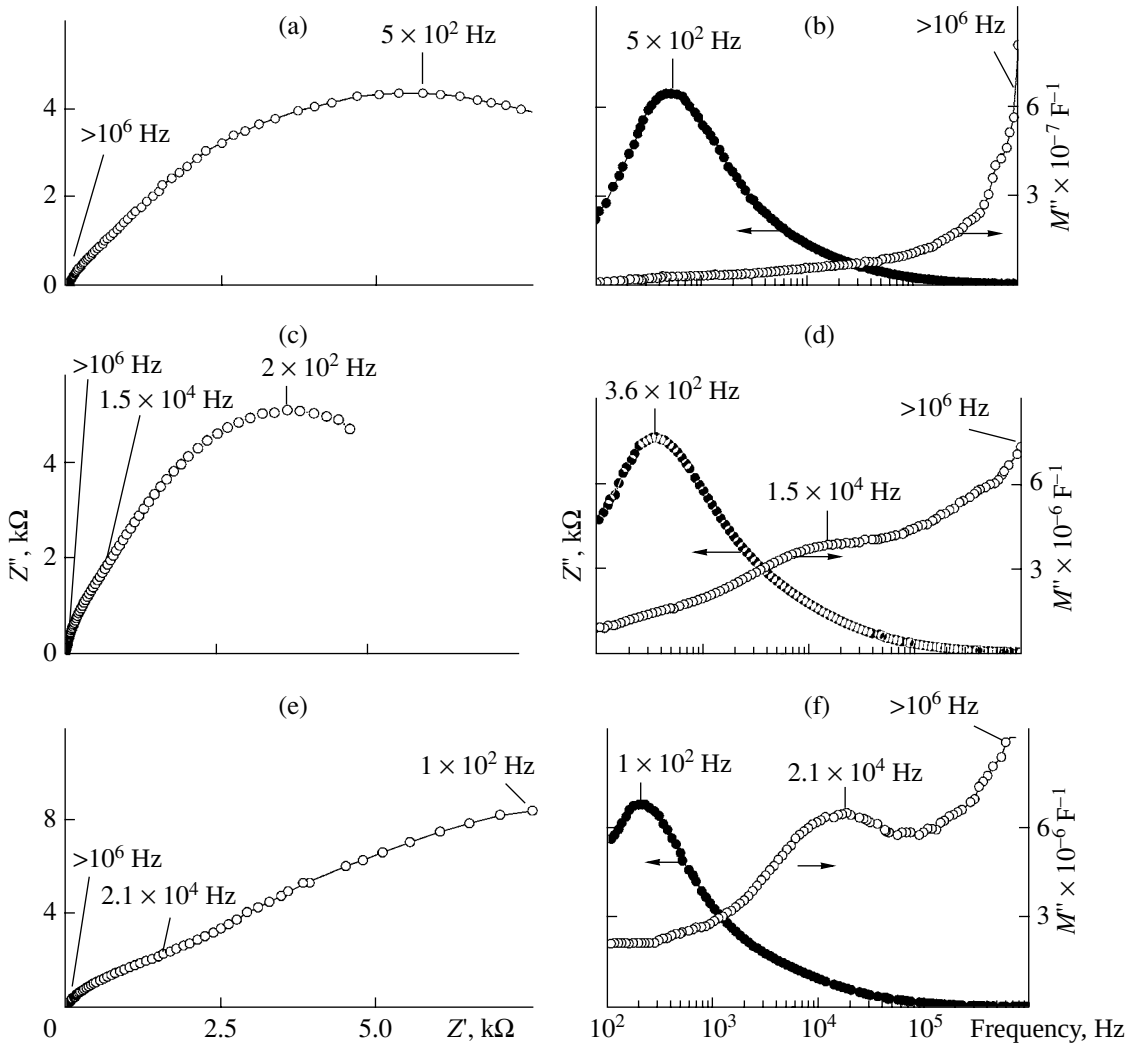

Fig. 4. (a, c, e) Nyquist diagrams and (b, d, f) frequency dependences of the imaginary part of impedance Z'' and electric modulus M'' for (a, b) $Ba_{0.99}Y_{0.01}Ti^{4+}_{0.99}Ti^{3+}_{0.01}O_3$, (c, d) $Ba_{0.975}Y_{0.025}Ti^{4+}_{0.975}Ti^{3+}_{0.025}O_3$, and (e, f) $Ba_{0.96}Y_{0.04}Ti^{4+}_{0.96}Ti^{3+}_{0.04}O_3$ samples oxidized at 1150°C in air; measurements at 220°C.

It follows from Eqs. (1) and (2) that

$$\omega_{max} = \frac{1}{RC}, \quad (3)$$

$$Z''_{max} = \frac{R}{2}, \quad (4)$$

$$M''_{max} = \frac{\varepsilon_0}{2C}. \quad (5)$$

Equations (3)–(5) show that the frequencies corresponding to Z''_{max} and M''_{max} depend on both R and C. It should be emphasized that the frequency dependences of Z''_{max} and M''_{max} are merely different representations of experimental data since these quantities are related by

$$M'' = \frac{\varepsilon_0 Z''}{C R}. \quad (6)$$

In this study, impedance measurements were made at 220°C, where the temperature coefficient of resistance is negative in both reduced and oxidized samples (Fig. 3). Figures 4 and 5 show the Nyquist diagrams $Z''(Z')$ and the frequency dependences of Z'' and M'' for samples with the nominal compositions $Ba_{0.99}Y_{0.01}Ti^{4+}_{0.99}Ti^{3+}_{0.01}O_3$ (I), $Ba_{0.975}Y_{0.025}Ti^{4+}_{0.975}Ti^{3+}_{0.025}O_3$ (II), and $Ba_{0.96}Y_{0.04}Ti^{4+}_{0.96}Ti^{3+}_{0.04}O_3$ (III) after air oxidation at 1150 and 1350°C, and the table lists some parameters of peaks in the Nyquist diagrams. Note that the Nyquist

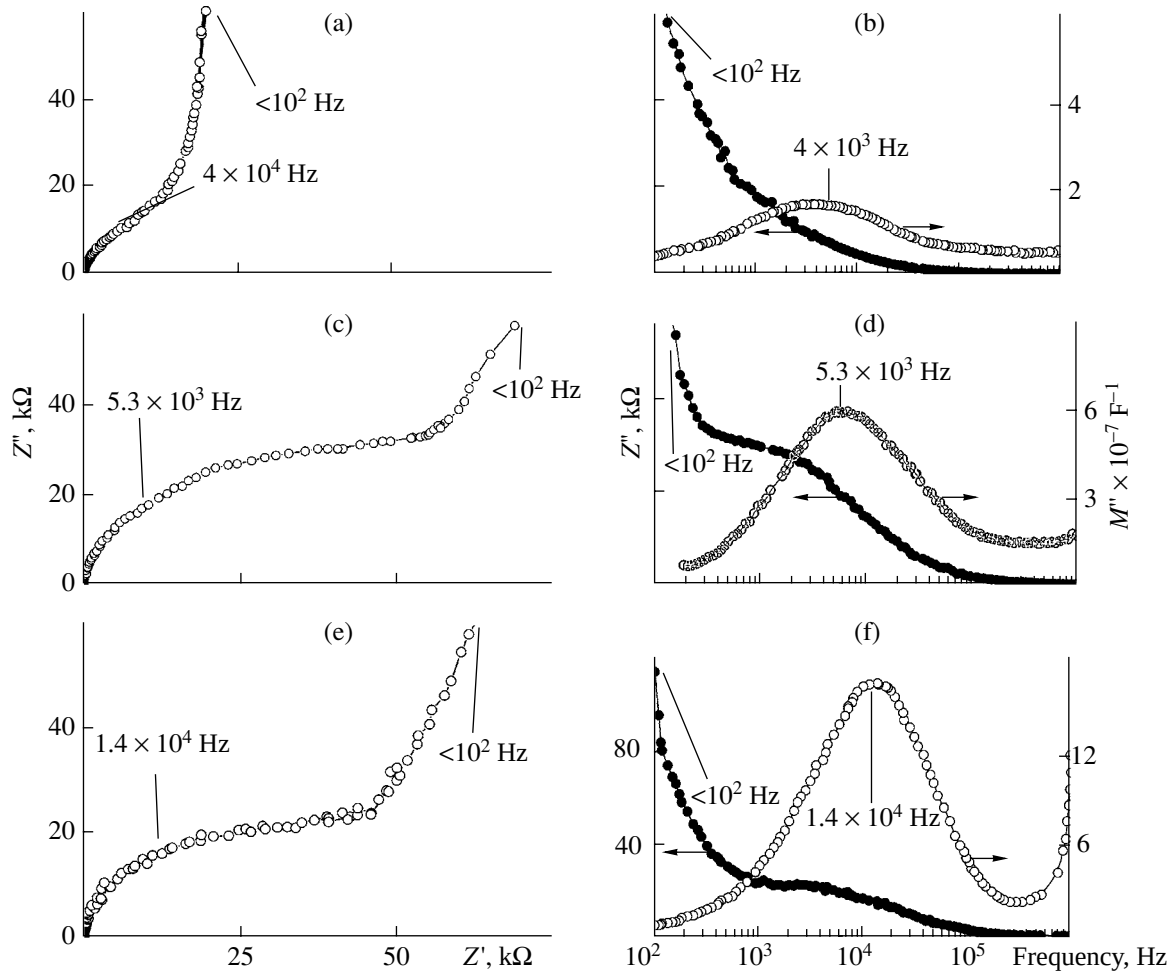

Fig. 5. (a, c, e) Nyquist diagrams and (b, d, f) frequency dependences of the imaginary part of impedance Z'' and electric modulus M'' for (a, b) $Ba_{0.99}Y_{0.01}Ti^{4+}_{0.99}Ti^{3+}_{0.01}O_3$, (c, d) $Ba_{0.975}Y_{0.025}Ti^{4+}_{0.975}Ti^{3+}_{0.025}O_3$, and (e, f) $Ba_{0.96}Y_{0.04}Ti^{4+}_{0.96}Ti^{3+}_{0.04}O_3$ samples oxidized at 1350°C in air; measurements at 220°C.

plots deviate from ideal semicircles, which can be taken into account by introducing constant-phase elements (CPEs). CPEs are often used to represent diffusion regions and are characterized by two parameters, Q and n, according to the formula $Z = Z_0/(i\omega)^n$. At $n = 1$, the CPE is equivalent to capacitance Q; n values below unity indicate that Q is frequency-dependent (dielectric dispersion) [23].

After oxidation at 1150°C, the $Z''(f)$ curves each show a single peak (Figs. 4b, 4d, 4f) at 500 (sample I), 400 (sample II), or 100 Hz (sample III), due to changes in the electrical properties of the dielectric grain boundaries. The $M''(f)$ curves of samples I–III show an increase in M'' around 1 MHz, suggesting that, at higher frequencies, there is a maximum due to the semiconducting properties of the grains (Fig. 4b). At the same time, increasing the Y content gives rise to an additional feature (at 15 kHz in Fig. 4d and at 21 kHz in Fig. 4f), due to changes in the electrical properties of the outer layer of the grains.

Similar behaviors of Z'' and M'' were revealed after air oxidation at 1350°C (Fig. 5). The oxidation rate at this temperature is faster than that at 1150°C, and the grain-boundary resistance reaches a higher level, which shows up as a shift of the peak in Z'' to lower frequencies (Fig. 5). In addition, the resistance of the outer layer increases, and its capacitance drops (table).

Thus, increasing the yttrium content of oxidized barium titanate markedly increases the resistance of the outer layer of the grains, which is attributable to the formation of $Ba_6Ti_{17}O_{40}$ and $Y_2Ti_2O_7$, revealed by XRD.

CONCLUSIONS

Oxidation of barium titanate doped with low yttrium concentrations leads to $Ba_6Ti_{17}O_{40}$ precipitation. At relatively high yttrium concentrations, both $Ba_6Ti_{17}O_{40}$ and $Y_2Ti_2O_7$ precipitate. The oxidation of reduced Y-doped barium titanate increases the resistance of the outer layer of its grains, the effect being stronger at

higher yttrium (donor impurity) concentrations and oxidation temperatures, which seems to be associated with the formation of $Ba_6Ti_{17}O_{40}$ and $Y_2Ti_2O_7$.

REFERENCES

1. Saburi, O., Properties of Semiconductive Barium Titanates, *J. Phys. Soc. Jpn.*, 1959, vol. 14, pp. 1159–1174.
2. Tennery, V.J. and Cook, R.L., Investigation of Rare-Earth Doped Barium Titanate, *J. Am. Ceram. Soc.*, 1961, vol. 44, no. 4, pp. 187–193.
3. Rotenberg, B.A. and Danilyuk, Yu.L., On the Nature of the Semiconducting Behavior of Barium Titanate, *Izv. Akad. Nauk SSSR, Ser. Fiz.*, 1967, vol. 31, no. 11, pp. 1824–1827.
4. Belous, A.G., V'yunov, O.I., and Khomenko, B.S., Microstructure and Semiconducting Properties of Barium Titanate Containing Heterovalent Substituents on the Titanium Site, *Neorg. Mater.*, 1998, vol. 34, no. 6, pp. 725–729 [*Inorg. Mater.* (Engl. Transl.), vol. 34, no. 6, pp. 597–601].
5. *Poluprovodniki na osnove titanata bariya* (Barium Titanate Semiconductors), Okazaki, M., Ed., Moscow: Energoizdat, 1982 (translated from Japanese).
6. Kröger, F.A., *The Chemistry of Imperfect Crystals*, Amsterdam: North-Holland, 1964. Translated under the title *Khimiya nesovershennykh kristallov*, Moscow: Mir, 1969.
7. Makovec, D. and Drofenik, M., Microstructural Changes during the Reduction/Reoxidation Process in Donor-Doped $BaTiO_3$ Ceramics, *J. Am. Ceram. Soc.*, 2000, vol. 83, no. 10, pp. 2593–2599.
8. Buskaglia, M.T., Buskaglia, V., Viviani, M., and Nanni, P., Atomistic Simulation of Dopant Incorporation in Barium Titanate, *J. Am. Ceram. Soc.*, 2001, vol. 84, no. 2, p. 412.
9. Kostikova, G.P. and Kostikov, Yu.P., *Khimicheskie protsessy pri legirovanii oksidov* (Chemical Processes in Doped Oxides), St. Petersburg, 1997.
10. Zhi, J., Chen, A., Zhi, Y., *et al.*, Incorporation of Yttrium in Barium Titanate Ceramics, *J. Am. Ceram. Soc.*, 1999, vol. 82, no. 5, pp. 1345–1348.
11. Belous, A.G., Preparation and Characterization of Ferro- and Antiferroelectric Metal Oxides and Their Potential for Microwave Applications, *Cand. Sci. (Eng.) Dissertation*, Moscow, 1978.
12. Evans, H.T., An X-ray Diffraction Study of Tetragonal Barium Titanate, *Acta Crystallogr.*, 1961, no. 14, pp. 1019–1026.
13. Kato, M. and Kubo, T., Solid State Reaction in the System of Y_2O_3–TiO_2, *J. Chem. Soc. Jpn.*, 1967, vol. 70, no. 6, pp. 840–843.
14. Negas, T., Roth, R.S., Parker, H.S., and Minor, D., Subsolidus Phase Relations in the $BaTiO_3$–TiO_2 System, *J. Solid State Chem.*, 1981, vol. 9, pp. 287–307.
15. Lines, M.E. and Glass, A.M., *Principles and Applications of Ferroelectrics and Related Materials*, Oxford: Clarendon, 2001, p. 112.
16. Okazaki, K., *Tekhnologiya keramicheskikh dielektrikov* (Ceramic Engineering for Dielectrics), Moscow: Energiya, 1976 (translated from Japanese).
17. Iton, J., Park, D.-C., Ohashi, N., *et al.*, Oxygen Defects Related to Electrical Properties of La-Doped $BaTiO_3$, *Jpn. J. Appl. Phys., Part 1*, 2002, vol. 41, no. 6A, pp. 3798–3803.
18. Sinclair, D.C., Morrison, F.D., and West, A.R., Applications of Combined Impedance and Electric Modulus Spectroscopy To Characterise Electroceramics, *Int. Ceram.*, 2000, vol. 2, pp. 33–37.
19. Morrison, F.D., Sinclair, D.C., and West, A.R., An Alternative Explanation for the Origin of the Resistivity Anomaly in La-Doped $BaTiO_3$, *J. Am. Ceram. Soc.*, 2001, vol. 84, no. 2, pp. 474–476.
20. Morrison, F.D., Sinclair, D.C., and West, A.R., Characterization of Lanthanum-Doped Barium Titanate Ceramics Using Impedance Spectroscopy, *J. Am. Ceram. Soc.*, 2001, vol. 84, no. 3, pp. 531–538.
21. Jonker, G.H., Some Aspects of Semiconducting Barium Titanate, *Solid-State Electron.*, 1964, vol. 7, pp. 895–903.
22. Dutta, P.K. and Alim, M.A., The AC Electrical Behavior of Hydrothermally Synthesized Barium Titanate Ceramics, *Jpn. J. Appl. Phys., Part 1*, 1996, vol. 35, no. 12, pp. 6145–6152.
23. Macdonald, J.R., *Impedance Spectroscopy*, New York: Wiley, 1987, p. 27.